ADVANCED FUNCTIONAL MATERIALS
www.afm-journal.de

Materials Views
www.MaterialsViews.com

Scanning Probe Microscopy of Nanocomposite Membranes and Dynamic Organization

Gabriel A. Montaño, Peter G. Adams, Xiaoyin Xiao, and Peter M. Goodwin*

Nanocomposite membrane assemblies are a class of materials that incorporate inorganic/organic nanoscale materials, such as fullerenes and gold nanoparticles or nanostructured materials with bio-inspired amphiphilic structures composed of molecules such as lipids or block copolymers. One of the intrigues of such materials is the potential to develop programmable membrane assemblies that mimic biological membrane complexity, dynamics and function. Due to the nanoscale nature of the assemblies, it becomes necessary to understand interactions between these materials with nanoscale resolution. Although many techniques are able to provide information as to the overall organization of membrane-based assemblies, only scanning probe microscopy (SPM) methods allow for a direct visualization of stochastic processes under environmentally relevant conditions. Here, an overview of nanocomposite membrane and thin film architecture investigations is presented with an emphasis on using in situ atomic force microscopy (AFM) in combination with fluorescence microscopy/spectroscopy techniques to understand organization and dynamics, in relation to activities and capabilities at the Center for Integrated Nanotechnologies.

1. Introduction

Scanning probe microscopies (SPM) and in particular atomic force microscopy (AFM) have proven to be critical techniques in investigating soft materials including biological and bio-inspired systems. The AFM was invented in 1985 by Binnig, Quate, and Gerber.[1] Amongst the key advantages to utilizing AFM in investigating soft-materials is that, in general, it is possible to perform high-resolution imaging under conditions conducive to soft and biological materials such as in liquid and without presence of a vacuum. A schemtic of the AFM is shown in **Scheme 1**. Further, it is possible not only to obtain high-resolution images but to measure properties such as mechanistic response and dynamic organization and perform nanomanipulation.

Dr. G. A. Montaño, Dr. P. G. Adams, Dr. P. M. Goodwin
Center for Integrated Nanotechnologies
Los Alamos National Laboratory
Los Alamos, NM 87545, USA
E-mail: gbmon@lanl.gov
Dr. X. Xiao
Sandia National Laboratories
P .O. Box 5800, Albuquerque, NM 87185, USA

DOI: 10.1002/adfm.201203429

There is an extensive literature and numerous reviews focused on various aspects of scanning probe microscopy techniques and biological/soft materials. It is not the goal of this review to provide an exhaustive description of SPM and soft/biological materials, but rather to focus on the use of atomic force microscopy in conjunction with other techniques as a means for investigating nanocomposite membrane assemblies with a focus on work being performed at the Center for Integrated Nanotechnologies. In context of this review, nanocomposite membrane assemblies are described as biological, bio-inspired or bio-hybrid, amphipathic structures that interact with nanostructured or nanoscaled materials. As described in more detail below, such materials have interest for a variety of applications, however as a field, much remains to understand in order to exploit the potential of such organized materials.

1.1. Atomic Force Microscopy and Bio-Membrane Investigations

Soon after the invention of AFM, investigations of membrane-like architectures began appearing in the literature.[2,3] Over the next two decades, thousands of papers have appeared in the literature using AFM to investigate biological, bio-inspired and bio-hybrid membranes. A large amount of work has focused on refining imaging techniques and strategies toward obtaining high-resolution images of 2D organized membrane structures.[4–8] Others have sought to use the AFM probe as a nanomechanical tool in membrane research.[2,9,10,11–13] With improvements in AFM instrumentation, probe manufacturing and development of combined systems with other forms of microscopy and spectroscopy, AFM has become one of the preeminent techniques in investigating 2D membrane assemblies. In particular, development of AC-mode techniques (also known as, 'tapping mode AFM') resulted in an avalanche of in situ AFM of soft materials, including membrane-based composite materials.[14,15] These advances allowed for obtaining high-resolution images of soft/biological materials that were previously only possible using techniques such as electron microscopy. AFM is not limited to ordered structures, unlike diffraction techniques, and can achieve nanometer resolution of diverse, disordered membrane architectures. AFM has

the added advantage of working under liquids, in biologically relevant or environmentally controlled conditions without the need for any desiccation or staining of samples. High-resolution AFM imaging has resulted in characterization of a number of membrane-protein 2D structures[8,13,16]and in some cases dynamic behavior of such systems[6,8,9,13] helping determine mechanisms of membrane-based organizations. However, AFM has also proven to be effective as a nanoscopic tool of membranes, capable of performing measurements of mechanics, such as force and elasticity[11,12,14,17,18] as well as a tool for nanomanipulation.[7,9,11,19]

1.2. Membrane Complexity and Bio-Inspired Assemblies

Our understanding of the biological membrane, particularly its organization and dynamics has been extensively refined recently.[20] The classic fluid mosaic model that described a randomized milieu of probability has been replaced by a model that describes a more programmed, directed assembly of materials that responds to external shifts such as presence of molecules that bind and environmental pressures. AFM has contributed to this understanding, allowing observation of biological membrane proteins in their native, imperfectly ordered organizations, often forming densely-packed functional protein domains.[5,21,22] For example, in biological membranes involved in photosynthesis, AFM has revealed adaptive changes in protein organization in response to specific genetic mutations[23] and altered cell growth conditions.[6,24] Biological membranes are now thought to exhibit complex, dynamic organizations that result in the variety and complexity of function.

It is within this intrinsic complexity of function and dynamics that the desire to understand and mimic membrane-based composites has arisen. Model bilayer systems

Gabriel A. Montaño is a Technical Staff Member with the Center for Integrated Nanotechnologies (CINT) at Los Alamos National Laboratory (LANL) and leads the Programmable Membrane–Based Nanocomposites Integrated Focus Area. He received his PhD working with Dr. Robert Blankenship at Arizona State University in 2002 investigating green–bacterial light–harvesting complexes. He followed as an Intelligence Community Postdoctoral Fellow at LANL with Dr. Andrew Shreve focusing on membrane–based biomimetic materials assemblies prior to joining CINT.

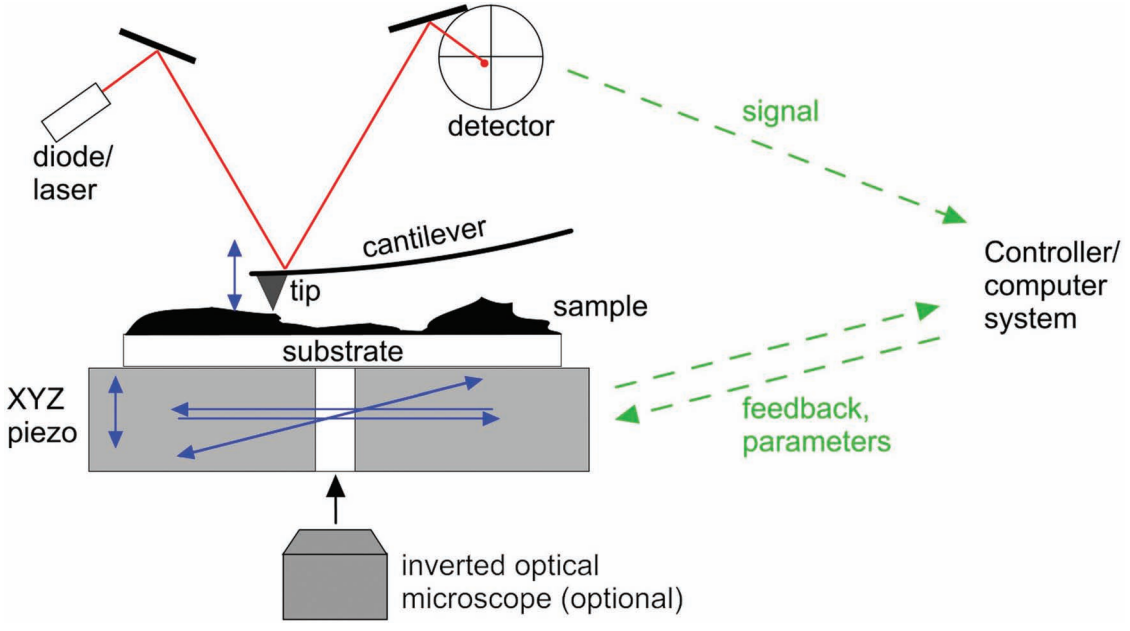

Scheme 1. Schematic of the atomic force microscope. An AFM probe is comprised of a sharp tip at the end of a flexible cantilever. This probe is raster-scanned across the sample, in physical contact with the sample surface and the deflection (bend) of the cantilever due to its interaction with the sample is monitored by a diode or laser, which is reflected off the back of the cantilever onto a position-sensitive photo-detector. A topograph is built up line-by-line from the inferred height. Samples are adsorbed onto a flat substrate, such as mica, glass or gold, and mounted on an XYZ piezo-electric scanning stage. The sample is scanned using the xy-piezo, and a computer-controlled feedback system adjusts the vertical position of the sample via the z-piezo, to maintain the close tracking of the probe. The operator adjusts imaging parameters on the computer interface as necessary to acquire a high quality image. Some AFM setups are combined with an inverted optical microscope, as described in Section 4, allowing correlated height and fluorescence images.

provide a scaffold on which it is possible to investigate cellular mechanisms such as lipid dynamics, and lipid environmental response.[25–27] Further, due to their amphiphilic nature, membrane-based nanocomposites are capable of serving as scaffolds for amphiphilic and hydrophobic materials such as membrane proteins and synthetic, hydrophobic or amphiphilic materials. Thus, lipid-based membrane assemblies have been used to investigate ligand-receptor interaction,[28] cellular signaling,[17,29] and energy transduction properties[22,30] as well as organization and coordination of synthetic nanomaterials. Interactions with nanomaterials has been a recent hotbed of activity particularly in context of nanotoxicity or health and biological effects of nanoparticles. Since the membrane serves as the point of interaction with any external material, membrane-based assemblies serve as model structures for understanding this first level of interaction. For reviews on recent advances in AFM of lipid bilayer assemblies see refs. [31,32].

Membrane-based nanocomposite materials are not limited to lipid-based structures. The idea of generating a barrier can be extended to other materials such as amphiphilic block-copolymers and grafted polymer assemblies.[33–40] In many ways, polymeric-based membrane assemblies provide significant advantages over lipid-based assemblies. Polymers are 1) robust, 2) tunable and 3) can exhibit dynamic shifts in 3D properties if properly designed. There has been a significant increase in investigations of polymer-based membrane composites. Further, nanocomposites are not limited to synthetic nanoparticles interacting with membrane structures. Nanotextured substrates have served as scaffolds for membrane materials and are discussed herein. These surfaces can consist of lithographically patterned or chemically functionalized substrates.

In this review, we discuss investigations of membrane-based nanocomposites using AFM in combination with other techniques, with a particular emphasis on work performed at the Center for Integrated Nanotechnologies User Facility (CINT). Examples of both lipid and polymer-based membrane nanocomposites are described. A further emphasis is placed on investigating dynamic behavior in membrane-composite materials. AFM, when used in conjunction with other techniques can be effective at developing models for dynamic organization and response. This is a focus of research described within this review. A further discussion is provided on current and future endeavors within CINT as part of an Integration Focus Area (IFA) on investigating programmable membrane-based nanocomposite assemblies.

2. Lipid Membrane Organization and Dynamics via AFM

Lipid-based assemblies have dynamic organizations that are known to be fluid in nature to varying degrees. Depending on composition and environmental conditions, dynamic phase separation and membrane reorganization can also occur. Soon after the development of AC-mode AFM, Gaub et al. reported observing lipid bilayer degradation via the A2 lipase.[41] This work demonstrated the ability of using AFM as a dynamic tool in making quantitative assessments. In the case of Gaub et al., the authors analyzed the membrane deformations in context of enzyme activity and proposed that in essence, singular disruptions were the result of single enzyme activity. The authors also demonstrated how AFM interpretation in conjunction with other techniques, such as previously reported data and information known about PLA2, enhanced the ability to make quantitative conclusions using in situ AFM.

There has been an extensive amount of research performed in understanding lipid-based membrane dynamics via AFM (for a more thorough review on this topic see ref. [42]). Applications in cellular dynamics, membrane-based sensor design, hybrid films for energetics, etc. have been the focus of many such investigations. The ability to obtain nanoscopic to microscopic images, work in air and in liquid, and monitor on timescales ranging from minutes to days, makes AFM an ideal technique for investigating membrane-based dynamics. When used in conjunction with other techniques such as fluorescence microscopy and spectroscopy, elliposometry, etc., it becomes possible to gain detailed quantitative understanding of membrane dynamics.

2.1. pH Response of Membranes

The ability to adjust in situ conditions allows one to monitor environmental response of membrane-based assemblies. Understanding environmental effects on membrane dynamics is important for understanding potential cellular membrane effects as well as in design of biomimetic assemblies.[26,27,43] However, determining dynamics is often difficult and can require a combination of techniques. Multi-component lipid assemblies have been previously studied that indicated an ability to induce effects such as phase-separation (discussed in detail later) and 3D structure formation in response to environmental stimuli.[44] However, the effects to which one could generate similar assemblies using a single-lipid system had not been seen. Further, a lack of AFM results often made structural interpretations difficult in previous studies. Goertz et al. demonstrated that under extreme pH conditions it was possible to observe large deformations in a lipid membrane assembly consisting of only the lipid 1-palmitoyl-2-oleoyl-sn-glycero-3-phosphocholine (POPC). In cases of fluorescence microscopy, a fluorescent lipid dye analog was also added in order to visualize.[26] Under acidic conditions, bubbles formed that had the potential to leave the surface in the form of liposomes if low enough pH was used. (**Figure 1**) A combination of techniques including AFM was used to demonstrate the formation of holes resulting from the liposome formation and release. (Figure 1a,b) Previously, similar areas in mixed lipid systems were described as phase-separated areas in which dye analogs were excluded resulting in the observed dark patches.[45] Using AFM, however, Goertz et al. found the dark patch areas in their studies to be holes in the membranes, presumably resulting from the loss in lipid concenteration due to the observed bubble formation and popping. Under basic conditions, a different response in membrane behavior was observed. Fluorescence microscopy and confocal microscopy indicated that membranes initially delaminated from the surface and then formed 3D structures of varying size and complexity. Remarkably, these

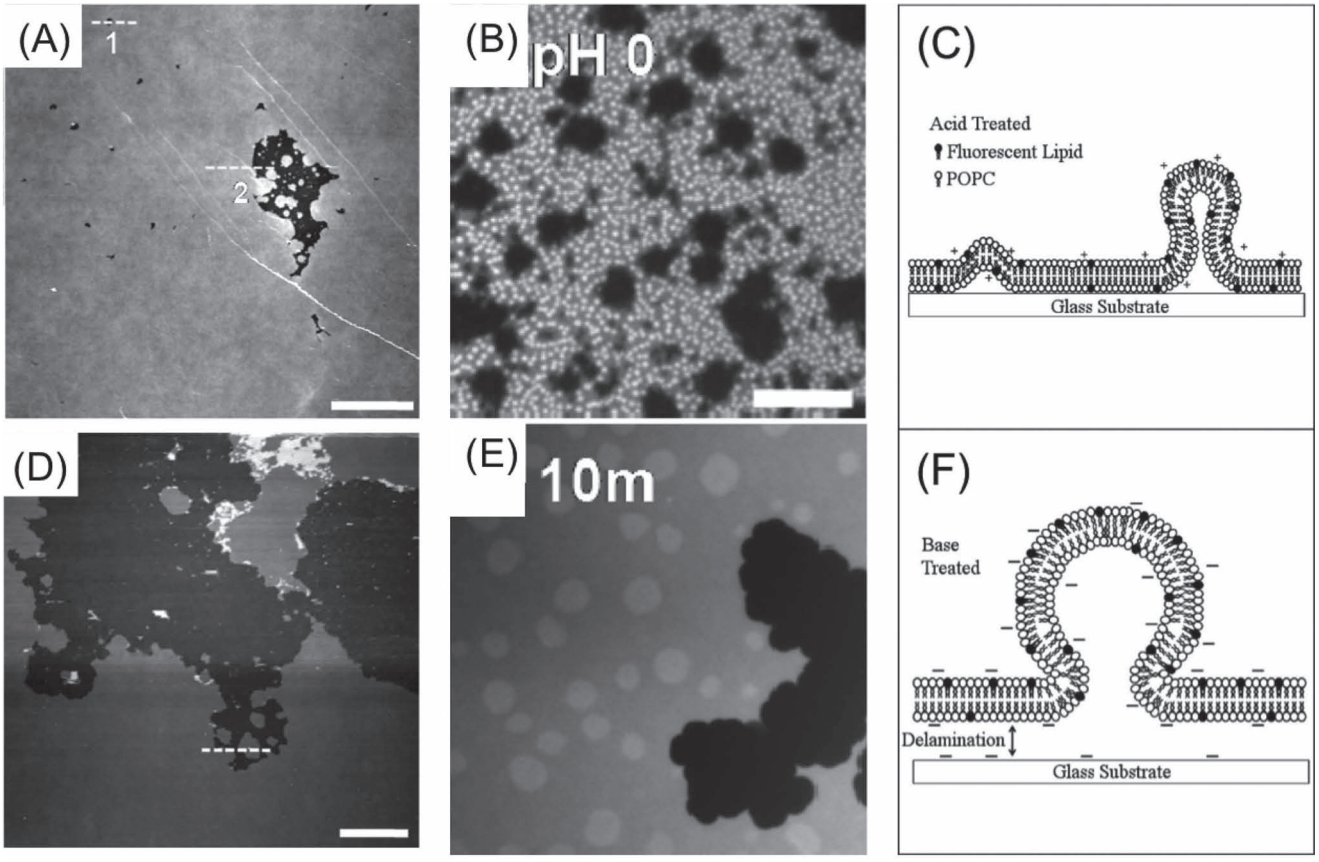

Figure 1. POPC LBAs in response to extreme pH conditions. a) AFM of POPC LBA at pH 1 (full z-scale = 6 nm; x-y scale bar = 5 µm); b) fluorescence image of POPC LBA at pH 0. (scale bar = 10 µm); d) AFM of POPC LBA at pH 13 (full z-scale = 10 nm; x-y scale bar = 5 µm); e) fluorescence image of POPC LBA at pH 12.5 (same scale as in (b)). Panels (a,b,d,e) adapted with permission.[26] Copyright 2012, American Chemical Society. c,f) Schematic depicting the mechanism of lipid bilayer reorganization under c) acidic and f) basic pH.

processes happened on the order of miliseconds to seconds. Also observed during the deformation were what appeared to be large deformations occurring in the membrane with ripping and reformation of the membrane occuring on a scale of tens of microns and on time scales of microseconds to seconds. Similar types of areas void of dye were also previously reported as areas described to be void of dye due to dye-specific segregation in lipid membranes.[45] Due to the speed of formation/reformation in this study, such an explanation also seemed plausible in these studies. However, AFM indicated that the deformations were in fact deformations occurring on a rapid time scale and not dye segregation. (Figure 1d,e) These studies indicated the usefulness of AFM in conjunction with other techniques in determining dynamic membrane reorganization. Further, results indicated the necessity of a technique such as AFM when interpreting effects such as membrane disruption/organization that can otherwise be misleading.

2.2. Membranes on Nanotextured Surfaces

Nanotextured surfaces have been used as membrane supports for membrane separation into discrete areas and as potential device support, such as in microfluidic channels.[46–49] A number of reports investigating lipid membrane interactions with nanostructured surfaces have recently been reported. Groves et al. determined lipid segregation occurred in membranes composed of lipid/cholesterol bilayer mixtures on rounded, nanostructured supports. The authors found that segregation was dependent on local curvature.[46] Lopez et al. also investigated muli-component bicelles on nanotextured surfaces consisting of high-aspect ratio ridges with nano-scaled dimensions.[49] **Figure 2**a,b shows AFM images of bicelles creating lipid membrane assemblies that 1) demonstrate the first example of a continuous lipid-bilayer assembly (LBAs) from bicelles and 2) indicate suspended LBAs that suspend the wells in the nanostructured surface. The ability to generate suspended LBAs has been a long sought after property, particularly as a platform to investigate membrane proteins and in biosensor and membrane segregation. Further, the supported nature of the membranes allows for the potential of rapid fluid exchange underneath each bilayer; in essence being able to potentially exchange fluid and materials on either side of a supported lipid bilayer assembly.

Werner et al. also investigated lipid bilayer assemblies on nanstructured surfaces. These investigations focused on the

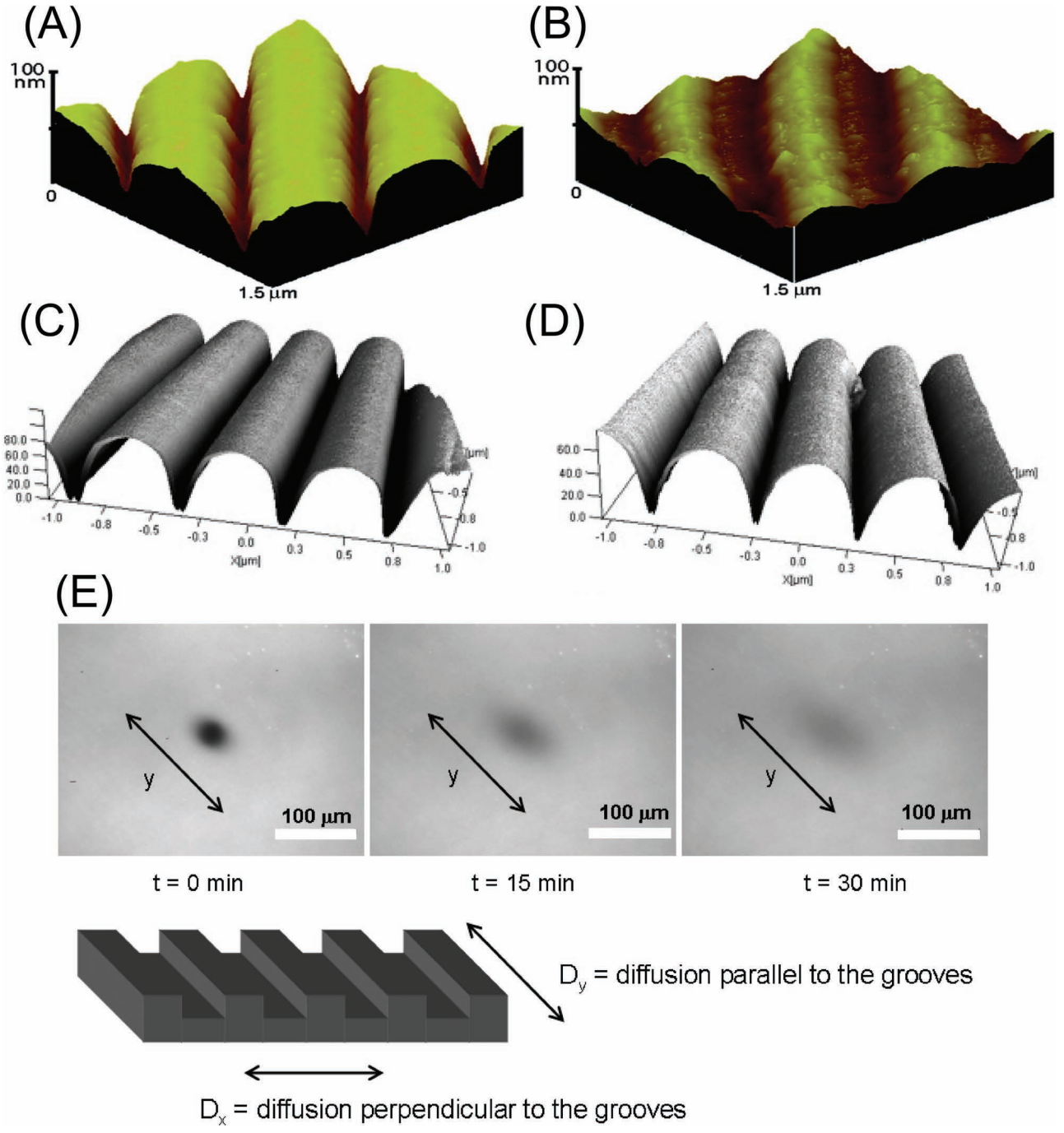

Figure 2. Lipid bilayer assemblies (LBAs) on nanotextured substrates shown from 3D representations of AFM data, x, y, and z dimensions labelled. a) AFM of nanotextured substrate prior addition of lipid bicelles. b) Nanotextured substrate after addition of lipid bicelles. c) AFM of nanotextured substrate prior to addition of POPC LBA. d) AFM of nanotextured substrate after addition of POPC LBA. E) FRAP indicating ellipsoidal recovery consistant with homogeneous recovery in both parallel and perpendicular directions as depicted. Figure adapted with permission.[48,49] Copyright 2006 and 2009, American Chemical Society.

membrane/substrate interactions and dynamic membrane formation with particular attention as to variations in membrane mobility due to surface curvature.[48] AFM was used to determine the nature of a POPC lipid bilayer association with the nanostructured substrate. As can be seen in Figure 2c,d, lipid bilayer assemblies were found to conform to the nanostructured surface. A width increase in the nanostructured ridges of ≈10 nm indicated bilayer formation on either side of the ridge. The high-aspect ratio of the nanostructured surface prevented AFM from determining LBA conforming throughout the wells of the structure. However, the lack of change in overall morhphology of the system indicated that coformation existed throughout

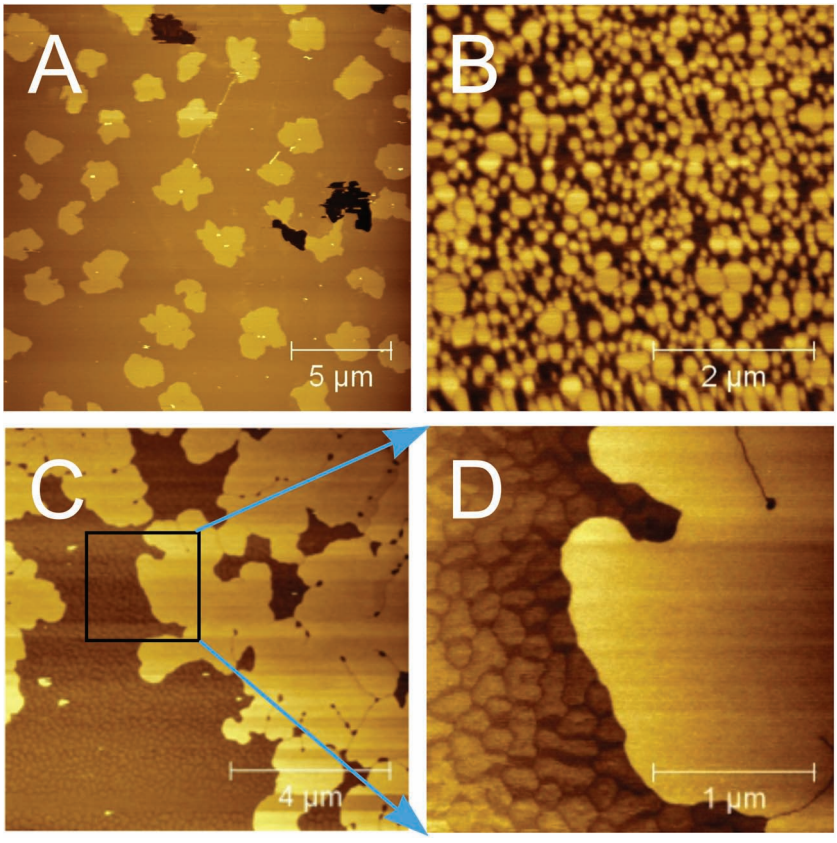

Figure 3. AFM images of phase separated lipid bilayers. Lipid composition: A) 40% DSPC and 60% POPC; B) 40% DOTAP and 60% DSPC; C,D) 80%DSPC and 20%DOTAP. Figure adapted with permission.[59] Copyright 2012 American Chemical Society.

the nanostructured surface. Fluorescence recovery after photobleaching (FRAP) verified the conforming nature showing an ellipsoidal recovery indicative of the bilayer traversing a greater distance in the direction of the ridges as opposed to the length of the ridges (Figure 2E). Simulations confirmed the experimental results indicating that local curvature effects played no part in membrane diffusion dynamics on these high-aspect ratio structures.

2.3. Lipid Bilayer Assemblies and Nanoparticle–Membrane Interaction

Atomic force microscopy (AFM) is a particularly informative technology to reveal biological membrane structures and structural changes corresponding to environmental variations, like interacting with foreign nanoparticles. AFM is capable of providing dynamic data sets with both high space (a few nanometers) and time (seconds) resolution, on domain formation, surface defects, adsorption, desorption, particle internalization, membrane disruption, etc.[50] Transmission electron microscopy (TEM) offers ultrasensitive information about the subcellular localization of nanoparticles but requires sample fixation and can only detect electron dense materials such as metallic nanoparticles but is not able to detect polymers, liposomes, and dendrimers easily.[51,52] Fluorescence microscopy is often used for live cell analysis with high time resolution but limited space sensitivity (submicrometer) to resolve detailed molecular interactions.

2.3.1. Nanostructured Phase Separation to Minimize Charge Repulsion

Soon after the discovery of AFM, it was widely applied to image biological molecules, such as single and double-stranded DNA, DNA nanostructures, proteins, protein-DNA assemblies, lipid bilayer membranes, etc. An advantage of AFM is that it can image nonconductive macromolecules on conductive and nonconductive substrates with single particle/molecule resolution.

Liposomes and supported lipid monolayers and bilayers are models to mimic cell membrane functions. The fluidity of a lipid bilayer depends on both its composition and temperature, as is readily demonstrated in studies of synthetic bilayers. A synthetic bilayer made from a single type of phospholipid changes from a liquid state to a two-dimensional rigid crystalline (gel) state at a characteristic freezing point. This change of state is called a phase transition, and the temperature at which it occurs is lower (that is, the membrane becomes more difficult to freeze) if the hydrocarbon chains are short or have double bonds. The short chain length reduces the tendency of the hydrocarbon tails to interact with one another, and cis-double bonds produce kinks in the hydrocarbon chains that make them more difficult to pack together, so that the membrane remains fluid at relatively low temperatures.

If composition of a LBA is varied, it can result in nano/microscopic phase separations that if imaged by AFM, can result in variations in, for example, LBA height. Though such variations may be as little as <1 nm, AFM is a useful technology for determining such subtle variations.

Figure 3A is an AFM image of the phase separation of a mixed bilayer consisting of POPC and distearylphosphatidyl choline (DSPC). POPC has a cis-double bond, while DSPC has two longer saturated alky chains. The image clearly shows two phases. The lighter islands of a variety of geometric shapes represent the gel phase DSPC in contrast to the darker fluid POPC. The kinked edges, or star shapes, indicate a rich dynamic lipid assembly and re-organization process during cooling. High-resolution images disclose uniform packing of lipid molecules in either fluid or gel phase domains showing no distinguishable nanostructures, respectively. Although the differences shown in Figure 3 appear to be dramatic, differences in height are on the scale of 0.5–2 nm.

When POPC is replaced by N-[1-(2,3dioleoyloxy)propyl]-N,N,N-trimethylammonium methylsulfate (DOTAP), which has a net positive charged headgroup, the domain sizes of gel

phase are significantly decreased to tens of nanometers. For example, a mixture of 40% DOTAP and 60% DSPC gives rise to domain sizes ≈ 50–150 nm (Figure 3B). These neutral domains of DSPC are separated from each other in order to maximize the separation of the charged fluid phases. In addition to the decreased domain sizes, nanostructures become apparent in the fluid phases with subnanometer resolution (Figure 3C,D). These nanostructures are observed very well at either high (>70%) and low (<40%) DSPC concentrations.[53] In between these two concentrations, the surface is mostly covered by small sized gel domains. The subnanometer nanostructures are due to leaflet mixing in DOTAP and DSPC bilayer structures, which could further maximum charge separation and expand the charge distribution. Such nanostructures diminish when adding POPC into the fluid phase of DOTAP, confirming that minimization of electrostatic repulsion is achieved by diluting the DOTAP package since POPC is mixed with DOTAP. The ability to obtain the detailed resolution of complex domain formations such as those described requires the resolution of AFM combined with the ability to image in environmentally controlled conditions indicating again the usefullness of in situ AFM in lipid membrane characterization.

2.3.2. Nanoparticle Assembling, Organization, and Membrane Pore Formation

The interaction of nanoparticles (NPs) with model lipid and cell membranes has been widely studied in recent years, since NPs have found promising applications as intracellular drug delivery agents, labeling in diagnostic imaging and biosensing, and cancer treatment, to name a few.[54] The growing use of the synthetic nanoparticles in industrial products such as cosmetics, processed food, drugs, etc. has raised serious concerns about potential toxic effects of nanoparticles on human health. The particle size, shape, surface functionality, hydrophobicity, surface charges, and softness are the important parameters affecting the particle interaction with membranes. Each parameter can have its own effect and interplays with other parameters for combined effects.[53,55,56]

It is generally agreed that the interaction of a nanoparticle to a membrane surface can be initiated by electrostatic attractions. Since biological cell membranes often have negative charges, positively charged nanoparticles, such as cationic monolayer-protected AuNPs, poly(L-lysine), cationic polymers, dendrimers, disrupt the membranes easily. When using lipid bilayers as model membranes, their surface charge and charge distribution can be controlled by mixing neutral and charged lipids. Further, in phase separated bilayer systems the surface charges can be localized to isolated phase domains.

LBAs can also be fluid materials and as described previously, can respond to environental stimuli. In a study by CINT investigators, the ability of NPs to adsorb to a lipid bilayer assembly was investigated.[57] Previous studies had indicated that rearrangement within a liposome allowed for zwitterionic lipids, such as POPC, to assume locally-charged patches of membrane that allowed for NP binding.[55] AFM results, however indicated that neither negatively or positively charged particles either bound to POPC LBAs nor were any observed patches of phase-separated lipid domains observed. However, when negatively charged particles were added to DOTAP LBAs, binding was observed. Further studies using Förster resonance energy transfer (FRET) based spectroscopy and localized lipid dye analogs revealed that the observed rearrangements reported by others are limited to non-supported lipid based arrangements such as liposomes and do not occur on surface supported systems. In order to verify this and eliminate curvature-induced effects, binding experiments were performed not only on flat substrates but also on silica spheres with diameters equivalent to prepared liposomes. Similar to the flat LBA systems, no evidence of binding or rearrangement was found.[57]

Other experiments also investigated the addition of charged NPs to LBAs. Over hours, AFM images did not show any particle adsorption or defect formation in supported lipid bilayers with net zero charges when AuNPs or CdSe quantum dots were introduced to the membranes. The observation was the same for both positively and negatively charged particles, indicating that all particle collisions are elastic in the absence of electrostatic attractions and with substrate support. The other interactions, such as hydrogen bonding, are not strong enough to bring the particle close enough to the LBA or eliminate the hydration layers of water around the hydrophilic lipid headgroups.[57–59]

Another study found that the surface charge density of monolayer-protected AuNPs played a significant role in their interaction with charged bilayer membranes. AuNPs coated with a pure monolayer of carboxylic acid terminals, so-called fully negative charged, often disrupt positively charged bilayers (even slightly charged) without adsorption. We assume that these particles collide at the surface and attract oppositely charged lipids with sufficient force as to disrupt the membrane.[59] Since the NPs are fully charged, they are quite soluble. This as well may play a role in the result of membrane disruption as opposed to membrane binding.

However, if one properly tunes both the membrane and the NPs, it is possible to use the fluidic and environmentally responsive nature of LBAs to organize NPs into nano-ordered structures. The surface charge density at AuNPs can be tuned by partially replacing negatively charged ligands with neutral ones. At ≈4:1 ratio of neutral:charged ligands, it was determined that particles could be adsorbed at DOTAP bilayers with very high particle density. As shown in **Figure 4**A, each individual spot represents single AuNPs or their aggregates adsorbed on a DOTAP LBA. The distribution of particles was rather random but coverage was complete.[58]

It is desirable to not only bind but also to utilize the fluidity of the lipid bilayer to potentially organize nanoscale materials. In the case of the bound AuNPs, it was determined that that NP organization was possible by introduction of $ZrCl_4$ solution to the system. Addition of $ZrCl_4$ resulted in the formation of nanorings that were shown to exhibit some level of ring-size control based upon $ZrCl_4$ concentration. While addition of other metal ions that have high binding affinity to the carboxylic acid, such as $NiCl_2$, and $ZnCl_2$, induced clustering, only $ZrCl_4$ solution gave rise to localized, nanoring formation as shown in Figure 4B. The chelation of zirconium ions with AuNPs has led to two-dimensional re-organization of AuNPs. The average diameter of rings is about 200 nm but can be varied by $ZrCl_4$ concentration. Also, high-resolution AFM

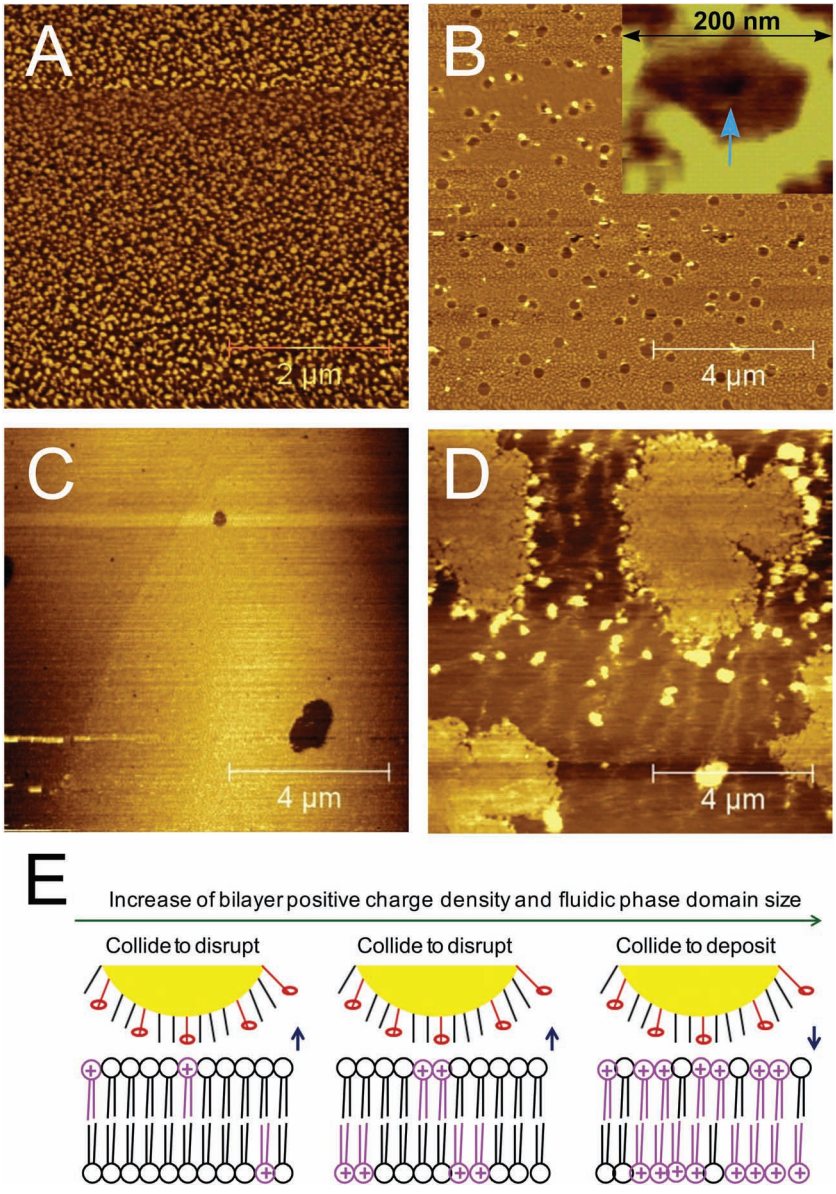

Figure 4. AFM images of AuNP interacting with LBAs. A) Partially carboxylated AuNPs on a covered DOTAP LBA before and B) after ziconiumm ion chelation reactions. The inset image showed a nanoring with membrane defects inside it. C,D) AFM images show selective membrane disruption. C) A fluid bilayer consisting of 10% of surface charge (90%POPC + 10%DOTAP) after introduction of oppositely charged AuNPs; D) severe disruption only occurs in fluid phases with positive charges (40%DSPC +30%POPC + 30%DOTAP). E) Schematics of the interactions between a partially negatively charged nanoparticle and a positively charged bilayer with increased local charge density and fluidic phase domain size (left to right). Figure adapted with permission.[58,59] Copyright 2011 and 2012, American Chemical Society.

images demonstrated that membrane defects were also formed inside the nanorings.[58] The nature of the reorganization was investigated and it could be explained by a mechanism involving both metal coordination and the previously described pH effects of membrane reorganization and disruption.[26,58] In brief, the Zr metal allowed for coordination of COOH groups on the Au NPs. This addition creates an aggregated network of Au clusters. However the addition of the $ZrCl_4$ also results in a substantial drop in pH (<pH2). As previously described, such a dramatic drop in pH can induce membrane reorganization, particularly bubbling or hole formation. Therefore, it is a combination of effects that results in the nanoring formation. The Zr coordinates AuNPs while at the same time causing membrane reorganization in the shape of bubbles. As the bubbles push away from the substrate, the AuNPs rearrange along with the membrane to form the ring structures that represent the outer diameter of the bubbles. When the lipidic bubbles leave the surface, a hole is left behind that is decorated by the nanoring. At higher concentrations of $ZrCl_4$ smaller ring diameters are observed. This is likely due to a more tightly packed coordination of NPs leaving less room for membrane deformation and hole formation. The increased concentration also causes a more dramatic drop in pH and thus the size of nanorings could also be somewhat kinetically driven as well. However, most important with these studies is the description of a system that relies upon the fluid nature of an LBA and its environmental response in order to allow for creation of synthetic nanoparticle assemblies.

2.3.3. Membrane Disruption Associated with Localized Surface Charges

Cell disruption is a process in which a cell membrane is perturbed to a degree that allows for loss of membrane viability in structure and function. The process is sensitive because different membranes have different structures, fluidity, surface charges, and functionalities. The most difficult samples to disrupt (e.g., spores) require mechanical forces combined with chemical or enzymatic efforts, often with limited disruption efficiency. Therefore, determining means for controlled disruption of membranes is desirable. Nanoparticles have exhibited properties in membrane disruption and in a potentially controllable, selective manner.

Charge density of the LBA and the NP can have an effect on interaction effects. Also, the ability to tune both the charge of the LBA and NP has been demonstrated. For example, the charge density and distribution inside the bilayer membrane can be tuned by varying the molar ratio of charged and neutral lipids in multicomponent membranes. The charge can also be localized in either fluid or gel domains. In previously described monolayer-protected NPs, the organic monolayer determines the nature of NP surface charge. Thus, it is possible to tune the charge distribution of a NP by controlling monolayer surface funtionality leading to a well-defined control of the charge and charge distribution.

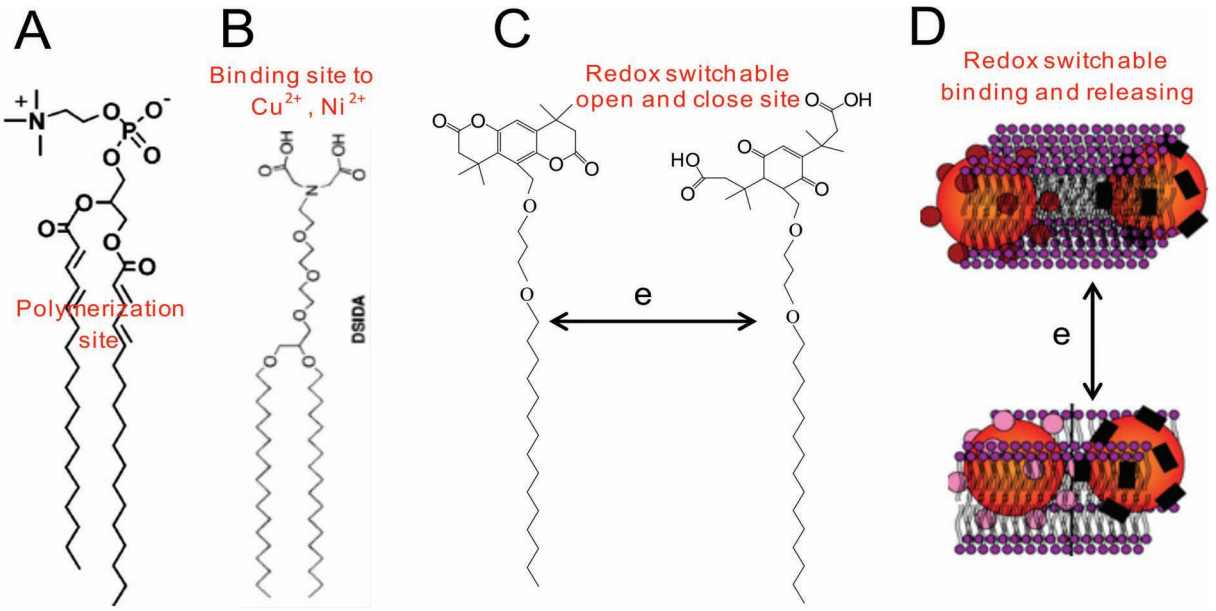

Figure 5. Representative chemical and electrochemical mechanisms used to control the membrane structures and the organization of nanoparticles inside the membranes.

In the absence of surface charges (100% POPC), AFM images indicate a lack of charged AuNP interaction, binding or defect formation. When the surface charge is altered by addition of 10% positively charged DOTAP, random defects begin to appear and increase in size with time as observable by dynamic in situ AFM. (Figure 4C).[59] The process is similar to a nucleation and growth process, indicating that the membranes are more easily disrupted at defect sites. Interestingly, no particles are observed to be adsorbed to the surface or are found while in the process of membrane disruption indicating the kinetics of the disruption mechanism are not within our typical scan rates of 1 Hz (line s^{-1}).

When the surface charge is further increased, massive membrane disruption is observed. This process was found to be charge localized as can be seen in Figure 4D. In this case the gel-phase areas composed of DSPC tightly pack exluding either of the fluid lipids POPC and DOTAP. Thus, membrane disruption is limited to the fluid areas where the DOTAP is present. The star shaped gel domains with net zero charge maintain their organization, while the fluid phases are severely disrupted. These experiments indicate the potential of NPs for inducing programmed membrane targeting and disruption as well as potential harmful effects of functionalized NPs interacting with cellular membranes.

2.4. Future Directions on Membrane Assembly and NP-Membrane Interaction

The extensive study of NP-membrane interaction is especially important in design of nanoparticles that avoid undesired side effects to biological cells. Model cell membranes offer advantages to study specific interactions of NPs and LBAs since their components, fluidity, and environments are precisely known and controllable. Proteins, polysaccharides, etc. adhere at the surface of cell membranes and biological media can overwhelm investigation of lipid/nanoparticle interactions.

LBAs can also be used as platforms for designer molecules in order to perform complex functions such as domain formation, recognition and binding events. For example, polymerization of synthetic lipids provide one-way tuning of the packing density of lipid membranes,[60] while two-way actuations can be obtained through chemical and electrochemical methods, such as metal ion chelation and redox processes. A synthetic lipid with an iminodiacetic acid headgroup, such as DSIDA shown in **Figure 5**B, can form uniform fluid bilayers with POPC. In the presence of copper ions, the chelation between copper ions and didactic headgroup brings the individual DSIDA molecules together to form gel-like microdomains. Such microdomains then sufficiently bind to TAMRA-labeled maltose binding protein with a 6-His tag (6-His MBP). Rapid reversibility of the system can be achieved by EDTA sequestration of metal ion from the membrane surface resulting in the release of bound protein and dissolution of the membrane domains, leading to a reversible switch between protein binding and release.[61]

The scheme shown in Figure 5C is one proposed mechanism being investigated to introduce a level of membrane dynamics control by oxidizing a neutral molecule to negative charges. Furthermore, the carboxylic acid terminals can provide potential routes of surface modification or directly coordinate with metal ions if desired. A wide range of host-guest reactions can also be applied to bring molecules or nanoparticles close together. An example is shown in Figure 5D. In the described case, one nanoparticle is terminated with ferrocene, while other is terminated with cyclodextrin. The neutral ferrocene can bind inside the cyclodextrin cavity while the charged ferrocenium

ion is expelled. Thus the spacing between the nanoparticles can be controlled as a function of the electrochemical oxidation and reduction of ferrocene. Such mechanisms for controlling dynamic membrane assembly and response are an avenue currently under investigation by members of our team.

3. Polymer Composite Nanomaterials and their Applications

Synthetic polymers offer many potential advantages for use in membrane nanocomposites, such as the ability to control chemical functionality and size, increased stability and decreased permeability. Polymers present different challenges than lipids, namely in the design of bio-compatible structures of the desired dimensions. Important considerations when choosing which polymer to use for an application include the chain length and monomers that constitute the chain. Short polymers may have a molecular weight of a few kDa, whereas long chain polymers can be significantly larger.

Considering chemical composition, homopolymers, where the chain is made up of only one type of monomer, contrast with heteropolymers, which contain two or more types of monomer. Block copolymers are a type of heteropolymer with two or more blocks of polymer covalently linked together, where each block is comprised of a single type of monomer. Polymers can be deposited onto a solid support to form thin films or even single layers. In blends of polymers in a thin film, self-association can take place to maximize favorable interactions and polymers of the same or similar type leading to formation of phase-separated domains. Where polymers are constrained, such as by linkage in block copolymers, 'microphase separation' can occur, producing domains on the nanometer scale.

By deposition of different polymers onto surfaces of different chemistries, a multitude of architectures can be formed. Many good reviews have looked at phase separation of polymers in detail.[35,36,52,62] Scanning electron microscopy has been used effectively in many studies to observe a variety of different microphase separations of block copolymers.[13,63] Where the surface of the polymer film is the focus of interest, scanning probe techniques are an ideal choice to visualize this domain formation, and the nanocompsite after deposition of structures on top of this film. AFM has the advantage of providing reliable 3D data of surface topography, mechanical data in phase contrast images and through force spectroscopy, and it is essentially non-destructive, if parameters are optimized (whilst electron microscopy may damage or alter polymer films).[36] This section of the review focuses on the use of polymer thin films to provide a nanoscale template for nanomaterials or alternatively the use of polymers as bio-mimics, and the utility of scanning probe microscopy to interrogate these nanocomposites.

3.1. Mixed Polymer Brushes and Nanocomposites

Polymer brushes are formations of polymers where the chains are attached to a surface at one end and stand up vertically, packing tightly together.[64] In mixed polymer brushes, more than one type of polymer brush is mixed on the surface to form a thin film. Polymer segregation can be limited by covalent attachment, or 'grafting', of one end of the brushes to a silicon substrate resulting in microphase separation and domain formation. Mixed polymer brushes of polystyrene (PS) and poly(methyl methacrylate) (PMMA)[65] and other mixed polymer brushes[66] have displayed reversible switching of the composition of the top brush as the microphase separation changed depending on the solvent. AFM revealed that exposure to a solvent selective for one polymer leads to a 'dimpled' top surface rich in that brush, whereas a non-selective surface leads to 'rippled' phases and formation of domains at the surface.[65] AFM nanomechanical measurements have demonstrated the differential elastic properties of domains in mixed polymer brushes when switching solvents.[67] The solvent-induced reversible switching of grafted diblock copolymer brushes has been harnessed to produce movement of silica nanoparticles across the surface.[68] Changes in the topography, as shown by AFM, were suggested to 'push' nanoparticles along, which lead to their agglomeration. If nanoparticle movement could be directed, as the authors note, one could envisage applications in nanotechnology.

Price et al. (2012), at CINT, recently produced the first in depth study of how microphase separation in mixed polymer brushes progressively changes dependent on the relative content of one brush to the other. Mixed polymer brushes were generated by random attachment of PS and PMMA homopolymers to a functionalized silicon surface in a series of different ratios of the two polymers, annealing in a non-selective solvent.[69] AFM revealed a sequential change in the nanodomain formation as the composition was varied from 0 to 68% PS (the remainder being PMMA): (i) small dimples of PS in a continuous matrix of PMMA (**Figure 6**A), to (ii) cylindrical domains of PS in a PMMA matrix (Figure 6B), to (iii) elongated 'rippled' phases of PS in a PMMA matrix (Figure 6C), to (iv) majority PS, where PMMA forms elongated 'rippled' phases in a PS matrix (Figure 6D). Different types of domain (hemispheres and cylinders) were found to coexist, creating a variety of patterns. The domain widths were measured to be 48 ± 5 nm. AFM topographs revealed that PMMA domains were slightly lower than PS domains (approx. 1 nm), whereas AFM phase images produced very clean domain boundaries based on the mechanical differences between the different polymer phases. Subsequent exposure of the mixed polymer brushes to solvents selective for either of the polymers allowed modulation of the nanodomain structure, increasing the size of the 'favoured' domains at the top surface. Computer simulations based upon self-consistent field theory produced qualitatively similar nanodomain structures once the probable non-uniform grafting density was taken into account. (Figure 6E–H) Relating simulations to experiments via the AFM data, indicates how the two approaches can be complementary. With knowledge of the progression in domain formation of grafted polymer brushes based on relative content of polymers, the effects of solvent selectivity and other factors, new nanocomposites can be designed and tuned.

3.2. Block Copolymers and Nanocomposites

Where one block of a diblock copolymer preferentially binds the surface, vertical phase separation can occur, forming layers

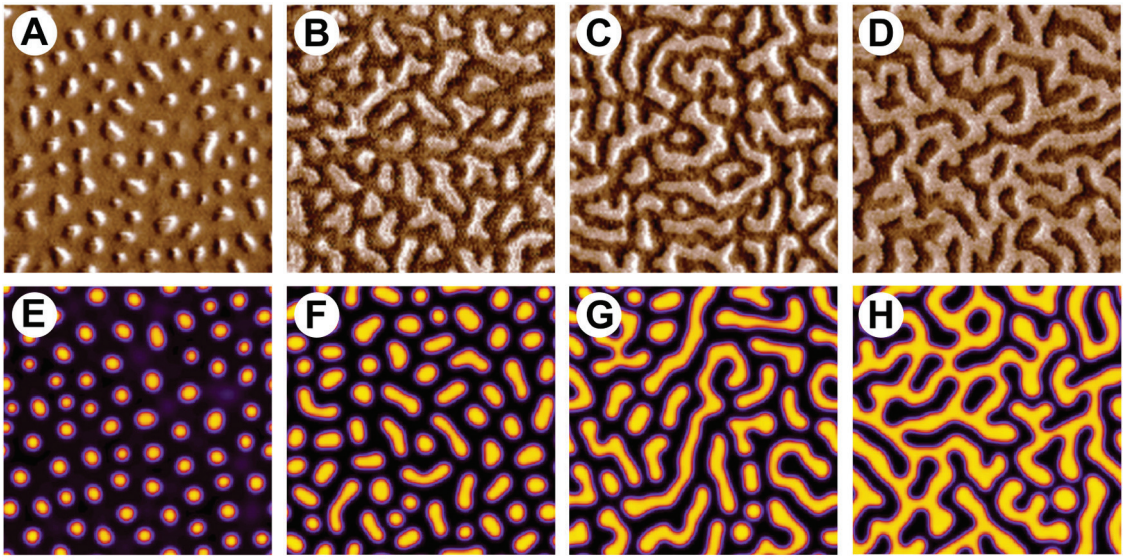

Figure 6. A–D) AFM phase images of the top surface of a thin film of PS and PMMA mixed polymer brushes on a functionalized silicon substrate, annealed in nonselective solvent vapor followed by a heat anneal. The volume fractions of PS in these samples was A) 0.38, B) 0.49, C) 0.51, and D) 0.58. Each panel is 1 μm × 1 μm. E–H) Self-consistent field theory phase images of the top surface of a simulated mixed polymer brush, with a number of equal length homopolymers A and B, each modeled as continuous Gaussian chains tethered to a hard, impenetrable surface. Simulations were performed with number fractions of homopolymer A of E) 0.1, F) 0.3, G) 0.4, and H) 0.5. Each box had height $3R_g$ and lateral dimensions of $(50 \times 50)R_g$ (where R_g = radius of gyration of the free polymer. Figure adapted with permission.[69] Copyright 2012, American Chemical Society.

of alternating self-associating polymer blocks, termed lamellar domains.[33] Ordered nanocomposites can be made from these formations, for example, gold and silicon dioxide nanoparticles have been shown to segregate within a vertically phase-separated blend of polystyrene-*block*-poly(ethylene propylene) (PS-*b*-PEP).[70] Transmission electron microscopy of cross sections cut through the film showed that gold nanoparticles segregated to the PS/PEP lamellar interface, whereas silicon nanoparticles were found within the PEP domains.[70] Alternatively, where there is no preference for either block of the copolymer, lateral phase separation can occur, leading to structures perpendicular to the surface, such as cylinders.[33] This produces patterns at the upper surface of the polymer film, such as arrays of dots, which could act as nanotemplates for arrangement of biological molecules.

Diblock copolymers of polystyrene-*block*-poly(methyl methacrylate) (PS-*b*-PMMA) have been investigated intensively because they have displayed good microphase separation and PMMA is readily photodegradable, allowing further nanofabrication processes. Channels through thin films, termed 'nanopores' can been formed by etching away the PMMA cylinders formed by laterally microphase separation in a PS-*b*-PMMA thin, shown with AFM.[71] Complex arrangements such as square patterns of pillars can be created by blending different block copolymers and multi-step etching processes.[72] Alternatively, the patterns generated by microphase separation can be exploited as templates for nanomaterials. Iron-platinum nanoparticles functionalised with oleic acid were selectively deposited onto the corrugations made from the UV-etching of PMMA domains from a laterally microphase separated thin film of PS-*b*-PMMA.[73] DNA molecules have been aligned on hexagonally patterned PMMA nanodomains on the surface of a laterally microphase separated PS-*b*-PMMA thin film.[74] By depositing the DNA in water and then simply drawing off the water with a pipette the receding water meniscus exerts forces that stretch out the long strands across the surface. This process, termed 'molecular combing', combined with the nanopattern of polymer domains, directed DNA strands to align along a row of the PMMA spots, as shown clearly in AFM images.[74] These DNA-polymer composites demonstrate a novel way to order fibrous molecules on a surface, with potential applications in gene-detection and nano-chip technologies.

Proteins have also been patterned onto similar nanotemplates. Kumar and Hahn[39] demonstrated that various proteins could be preferentially bound to PS domains in laterally microphase separated PS-*b*-PMMA. AFM topography and phase images showed that immunoglobulin G binds almost exclusively along the line domains of PS allowing formation of ≈45 nm wide 'nanochains' of tightly packed molecules. Further studies showed that biomolecules patterned onto these surfaces could retain their activity. Enzymes were active for over 100 days, enhanced green fluorescent protein was fluorescent and immunolabelling of patterned Protein G was successful.[75] Although only a small number of proteins have been patterned so far these results are promising.

3.3. Amphiphilic Block Copolymers Can Form Biomimetic Membranes

If a block copolymer is comprised of a hydrophilic block and a hydrophobic block it is possible to form structures that

resemble lipid bilayers, making use of vertical (lamellar) phase separation. Such low molecular weight, amphiphilic diblock copolymers self associate when put into water to sequester the hydrophobic blocks and expose the hydrophilic ones,[76] in an analogous way to lipids. Polymer micelles, polymer vesicles (termed 'polymersomes'), worm-like vesicles and multilayer vesicles can be formed, depending on the size of the hydrophilic block relative to the hydrophobic one.[77,78] Polymer vesicles in solution have been extensively investigated, showing that amphiphilic diblock copolymers can have advantages over lipids for design of nanocomposites, such as increased stability, decreased permeability, tunable response to external stimuli and their ability to encapsulate nanomaterials has been demonstrated.[77,79] Our focus in this review section will instead be placed on surface supported polymer bilayers. By a combination of AFM and other techniques these polymer membrane mimics can be effectively explored.

A surface supported polymer bilayer was first demonstrated by Belegrinou et al.[34] using PEO-*b*-PBD by Langmuir monolayer transfer from a water-air interface. The bilayer was covalently bound to a gold substrate by using sulphur-functionalised PEO. First, a monolayer was deposited by Langmuir–Blodgett transfer and then a second monolayer by Langmuir–Schaefer transfer, to form a smooth bilayer, confirmed by AFM. In a further study,[80] vesicles of the same sulphur-functionalised PEO-*b*-PBD were deposited onto a hydrophilic glass or gold substrate. However bilayers were not continuous and multilayers were formed as vesicles presumably deposited on top each other. Attempts to 'spread' out the vesicles using salt and elevated temperature improved the coverage but bilayers were not as 'clean' or continuous as those from Langmuir–Blodgett transfer. Triblock copolymers have also been shown to form biomimetic membranes with few defects.[38]

Goertz et al.[37] demonstrated that PEO-*b*-PBD micelles can be deposited onto glass substrates to form either monolayers or bilayers, depending on the surface functionality. When deposited in water onto hydrophilic piranha-cleaned glass the PEO favors the hydrophilic surface and a bilayer is formed in a sort of vertical phase separation, with polymer chains perpendicular to the surface, forming a hydrophilic-hydrophobic-hydrophilic sandwich, PEO-*b*-PBD-PBD-*b*-PEO. Deposition of the same micelles onto a hydrophobic surface of alkyl-functionalised glass resulted in a monolayer where the PBD associates with the surface and the PEO faces away, towards the aqueous milieu. The bilayers/monolayers were kept under water at all times, to maintain the hydrated conditions usual for biological systems. AFM topographs showed that these polymer layers are continuous, with a very low roughness (<0.5 nm) and essentially defect-free over many microns. By scratching away a square region by exerting deliberately high forces with the AFM tip and then reimaging with a larger scan size, the thickness of the polymer layer on the hydrophilic surface could be measured as 5nm, comparable to a lipid bilayer, and the polymer layer on the hydrophobic surface was measured at 2.5 nm, similar to a lipid monolayer. The authors also demonstrated the ability to create patterned hybrid polymer layers consisting of a continuous phase of silane-supported polymer monolayer and surface-supported polymer bilayer. AFM was able to determine the continuous nature of the hybrid membrane systems (**Figure 7**A,B). By attaching a fluorescent label to one end of the polymer, or by incorporating lipid-based dye molecules, the fluidity of the membranes was tested by fluorescence recovery after photobleaching (FRAP) experiments. In the hybrid systems, the bilayer regions were found to have very little mobility in contrast to monolayers which were at least 1000 times as mobile (no fluorescence recovery after 1 h, c.f., recovery after 10 min). (Figure 7D–F) This lack of mobility could be advantageous if one wanted to immobilize a membrane-associated protein or ligand such as Lipoarabinomannan (LAM) which is an amphiphilic critical virulence factor in the pathogenesis of Mycobacterium tuberculosis and readily inserts into lipid membranes,[28] the causative agent of tuberculosis, but not necessarily conducive to investigating functions requiring a fluid bilayer. For similar types of membrane-associated or inserting molecules, the methodology presented represents a potential path to simplified and robust array formation. These results indicated the ability to create physically discrete micropatterned membrane systems in a one-step approach. Interestingly, by drying out a PEO-*b*-PBD multilayer and then rehydrating the surface, the authors were able to create 'hollow hemispherical caps' with restored fluidity.[37] Future studies would do well to develop polymer based biomimetic membranes that are fluid, with potential to introduce membrane proteins into the polymer bilayer.

4. Combined AFM/Fluorescence Microscopy

Another area of recent development within CINT is a capability development in combined AFM and fluorescence microscopy. We have developed the capability for acquiring spatially registered AFM and fluorescence images. Briefly, this was accomplished by modification of a Bioscope SZ AFM (Bruker, formerly Veeco), that consists of an AFM scanner mounted on top of an inverted optical microscope (IX-71 Olympus). We modified the optical microscope for ultrasensitive, sample-scanned, confocal fluorescence imaging and single particle spectroscopy. Details of the system design can be found in ref. [81].

To collect the fluorescence image, the sample is raster scanned through the fixed excitation laser spot to generate the fluorescence image. The sample scan stage is then positioned at the center of the scanned region, and the AFM probe is engaged and scanned across the sample to produce an AFM height image as well as a spatial map of the excitation light scattered from the AFM probe. This scattered light image is then used to offset the AFM scan to align its center to that of the fluorescence image. Once aligned, a second, spatially registered AFM image is acquired. **Figure 8** shows three such images acquired from 100 nm diameter fluorescent beads dried onto a glass coverslip. Figure 8A shows the fluorescence image of the beads collected from a 10 μm × 10 μm region of the sample. Individual beads are visible as diffraction-limited spots. The brighter spots are two or more beads that are too close together to be resolved by the confocal microscope. Figure 8B shows the AFM height image of the same region. Individual polystyrene beads are clearly visible in this image and are well registered with the bead fluorescence shown in Figure 8A. Figure 8C is the spatial map of the excitation light scattered by the scanned AFM probe. As seen from this image the center of the AFM

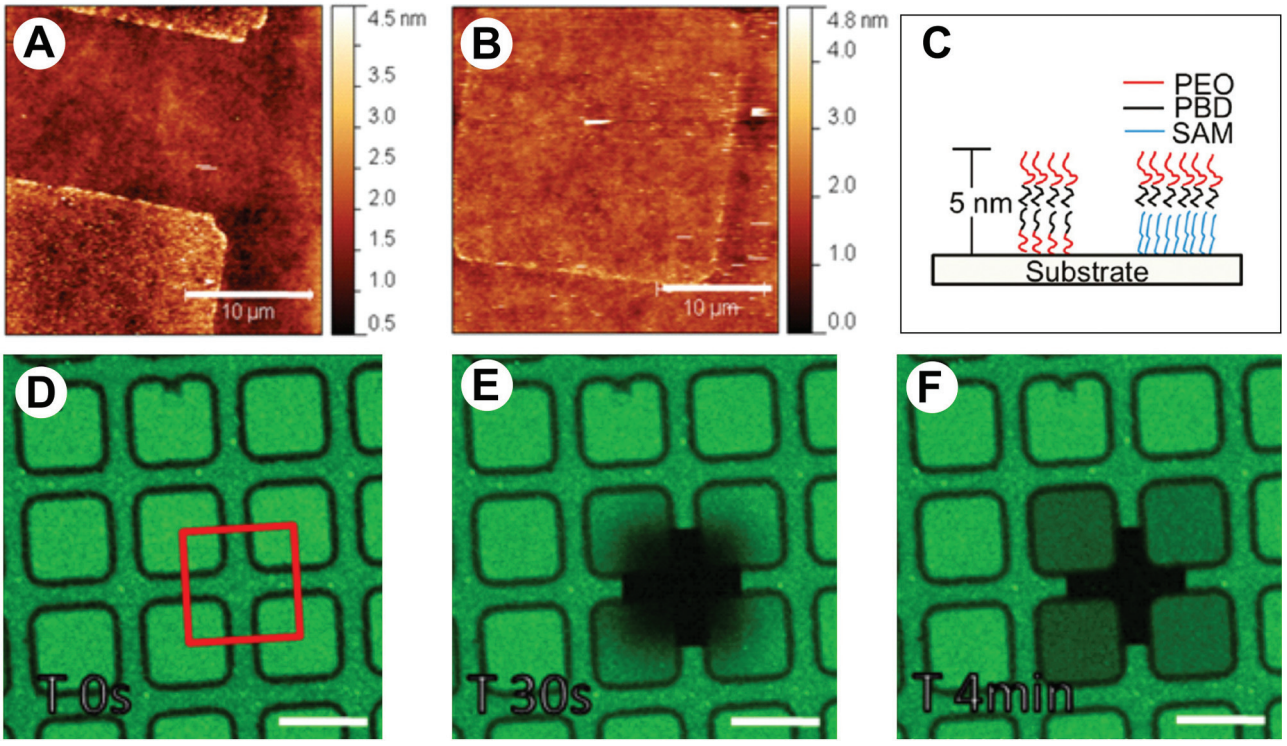

Figure 7. A,B) AFM topographs of hydrophilic glass after microcontact printing of a square pattern of a hydrophobic alkoxy silane, either A) before or B) after deposition of PEO-*b*-PBD micelles. C) Schematic representation of the conformation of PEO-b-PBD chains on a hydrophilic substrate (left) and hydrophobic silane (right). D,F) Fluorescence microscopy images of PEO-*b*-PBD micelles deposited on a microcontact printed glass, micelles labeled with C_{12}-BODIPY-lipids. Fluorescence recovery after photo-bleaching (FRAP) of a region shows the differential mobility of the polymers on different parts of the patterned surface. Time after bleaching (T) is shown. Scale bar = 20 µm. Figure adapted with permission.[37] Copyright 2012, American Chemical Society.

scan region is well aligned to the center of the sample stage scan region as is required for good registration of the fluorescence and AFM images.

The ability to generate spatially registered fluorescence and AFM images allows one to obtain chemical and spectroscopic information in addition to topological and mechanical information from the sample. We have an ongoing CINT project the goal of which is to characterize the topology (i.e., circular versus linear) of telomeric DNA. AFM will permit us to definitively determine the conformation of the telomeric DNA. Registered fluorescence and atomic force images of strand-specifically labeled telomeric DNA will allow us to further determine if the conformation of telomeric DNA is correlated with its mode of replication (i.e., leading- versus lagging-strand synthesis).

We tested the modified AFM setup by imaging double-stranded circular plasmid DNA (pKLAC1, 9091 bp) stained with the intercalating dye YOYO-1 at a 1:5 dye-to-base-pair ratio prior to immobilization on mica. Fluorescence was excited using

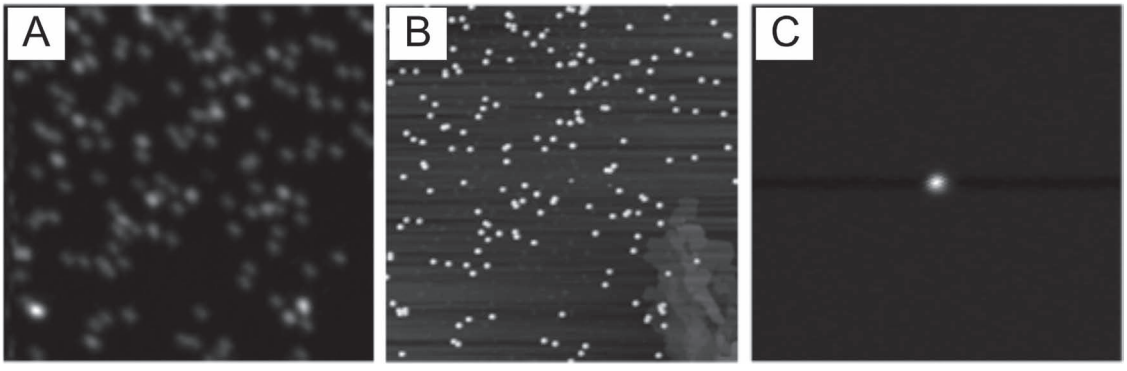

Figure 8. Spatially registered AFM and fluorescence images of 100 nm diameter fluorescent beads. A) Fluorescence image. B) AFM height image. C) AFM tip scatter map generated during the acquisition of the height image shown in (B). Image areas are 10 µm × 10 µm.

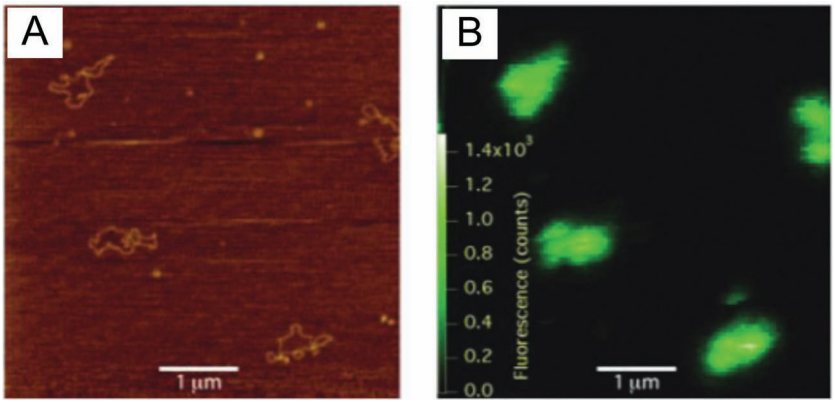

Figure 9. A) AFM height and B) fluorescence images of YOYO-1 stained plasmid DNA.

≈500 nW at 488 nm, and collected through a 50 nm band pass filter centered at 535 nm. **Figure 9** shows an AFM height image of four pKLAC1 DNA fragments, and the registered fluorescence image of the same region. YOYO-1 fluorescence detected from individual DNA loops is well above the background level (≈10 counts). The colorscale bar inset shows numbers of photons detected per pixel per 10 ms. Registration between the two images is not perfect, but is adequate to reliably assign fluorescence spots to individual DNA fragments. Diffraction-limited fluorescence image resolution prevents determination of DNA fragment topology (circular vs. linear) with certainty. In the AFM image, circular conformations of three complete fragments are readily apparent.

We have also used this setup to perform time-resolved single-particle spectroscopy of quantum dots (QD) and small ($n \leq \approx 5$) QD clusters.[81] Here the effective volume obtained from AFM height images of the individual nanoparticles provided the means to definitively differentiate between small QD clusters and isolated QDs.

5. Programmable Membrane Nanocompistes Focus Area at CINT and Future Directions

CINT has a dedicated Integration Focus Area (IFA) effort in programmable membrane nanocomposites. Scanning probe microscopy is playing a key role in current and future efforts and research designs. The focus of the Programmable Membrane-Based Nanocomposites (PMBN) Focus Area is to investigate the interactions between nanoscale materials and membrane-based composites such as lipid and polymer vesicles and membrane architectures. The ultimate goals of the research involves learning how to replicate many of the complex behaviors associated with cellular membranes within artificial nanocomposites and integrated systems. These integrated nanomaterials could be utilized in applications including electrical energy storage (the artificial electric eel), artificial photosynthesis, environmental remediation (reversible CO2 sequestration and water purification), and responsive sensors and adaptive materials. The starting point for understanding the behavior of complex membranes involves investigating the fundamental interactions between membrane hosts, nanoparticles, and substrate surfaces. Much of the described work is part of this IFA effort. Much of the work within the PMBN team has shifted to investigation of polymer-based membrane materials and nanoparticle interactions. These systems consist of grafted polymer systems and block copolymer based systems similar to those described in combination with functional substrates. Through CINT science and the CINT user program, these systems are being explored as platforms for electronic and photonic applications in particular. Further, fundamental research of nanoparticles with polymers and to some degree lipid based membrane systems is being performed, including: 1) nanoparticle adsorption, insertion, migration, and aggregation as a function of particle size, shape, and surface chemistry, 2) membrane responses as mediated by substrate interactions, including diffusion and transport, mechanical stability, domain formation and component partitioning, and 3) membrane-mediated nanoparticle organization.

Scanning probe microscopy is a valuable technique in being able to characterize the various properties of these new materials assemblies. While dynamic *in situ* AFM is an emphasis of work within the CINT PMBN team, utilizing capabilities in force spectroscopy has also become a recent focus. Further techniques such as Kelvin Force Probe Microscopy and Electrical Force Microscopy are also being used, particularly in evaluation of new composite materials based on conductive supports such as carbon nanotubes and graphene.

The development of membrane-based nanocomposites has been greatly advanced by scanning probe technology. In moving towards dynamic/responsive membrane-based composite materials it is necessary to understand and develop mechanisms of control on the nanoscale. Scanning probe allows for techniques to investigate organization and dynamics, interrogate properties such as localized electronics, mechanics and magnetics and manipulate materials on the nanoscale. Also, advancements made by members of our team in technique development such spatially registered AFM/fluorescence will allow for another advanced means of probing dynamic composite materials systems. As our capabilities in self-assembly and materials design improve, scanning probe technology and advancements in SPM will allow us to characterize these next generation of materials.

Acknowledgements

This work was performed, in part, at the Center for Integrated Nanotechnologies, a U.S. Department of Energy, Office of Basic Energy Sciences user facility. Los Alamos National Laboratory, an affirmative action equal opportunity employer, is operated by Los Alamos National Security, LLC, for the National Nuclear Security Administration of the U.S. Department of Energy under contract DE-AC52-06NA25396. We thank Dr. Susan M. Brozik and Dr. David R. Wheeler for discussion and support and use their schematic, Figure 5.

Received: November 21, 2012
Revised: January 28, 2013
Published online: April 8, 2013

[1] G. Binnig, C. F. Quate, C. Gerber, *Phys. Rev. Lett.* **1986**, *56*, 930.
[2] S. L. Brandow, D. C. Turner, B. R. Ratna, B. P. Gaber, *Biophys. J.* **1993**, *64*, 898.
[3] a) H. J. Butt, C. B. Prater, P. K. Hansma, *J. Vac. Sci. Technol., B: Microelectron. Nanometer Struct.* **1991**, *9*, 1193; b) J. Yang, L. K. Tamm, T. W. Tillack, Z. Shao, *J. Mol. Biol.* **1993**, *229*, 286.
[4] a) D. M. Czajkowsky, H. Iwamoto, T. L. Cover, Z. Shao, *Proc. Natl. Acad. Sci. USA* **1999**, *96*, 2001; b) S. Jaroslawski, K. Duquesne, J. N. Sturgis, S. Scheuring, *Mol. Microbiol.* **2009**, *74*, 1211; c) S. Scheuring, D. J. Mueller, H. Stahlberg, H.-A. Engel, *Eur. Biophys. J.* **2002**, *31*, 172; d) H. Seelert, A. Poetsch, N. A. Dencher, A. Engel, H. Stahlberg, D. J. Muller, *Nature* **2000**, *405*, 418.
[5] a) D. Fotiadis, Y. Liang, S. Filipek, D. A. Saperstein, A. Engel, K. Palczewski, *Nature* **2003**, *421*, 127; b) N. Buzhynskyy, P. Sens, F. Behar-Cohen, S. Scheuring, *New J. Phys.* **2011**, *13*, 085016.
[6] S. Scheuring, J. N. Sturgis, *Science* **2005**, *309*, 484.
[7] D. Fotiadis, P. Qian, A. Philippsen, P. A. Bullough, A. Engel, C. N. Hunter, *J. Biol. Chem.* **2004**, *279*, 2063.
[8] H. Yamashita, K. Voitchovsky, T. Uchihashi, S. A. Contera, J. F. Ryan, T. Ando, *J. Struct. Biol.* **2009**, *167*, 153.
[9] Y. F. Dufrene, *Nat. Rev. Microbiol.* **2008**, *6*, 674.
[10] a) D. Fotiadis, S. Scheuring, S. A. Muller, A. Engel, *Micron* **2002**, *33*, 385; b) A. Ikai, R. Afrin, A. Itoh, H. C. Thogersen, Y. Hayashi, T. Osada, *Colloids Surf., B* **2002**, *23*, 165; c) D. A. Cisneros, D. Oesterhelt, D. J. Mueller, *Structure* **2005**, *13*, 235.
[11] A. Ikai, R. Afrin, *Cell Biochem. Biophys.* **2003**, *39*, 257.
[12] M. Yokokawa, K. Takeyasu, S. H. Yoshimura, *J. Microsc.* **2008**, *232*, 82.
[13] E. W. Edwards, M. Muller, M. P. Stoykovich, H. H. Solak, J. J. de Pablo, P. F. Nealey, *Macromolecules* **2007**, *40*, 90.
[14] M. E. McConney, S. Singamaneni, V. V. Tsukruk, *Polym. Rev.* **2010**, *50*, 235.
[15] A. L. Klyszejko, S. Shastri, S. A. Mari, H. Grubmueller, D. J. Muller, C. Glaubitz, *J. Mol. Biol.* **2008**, *376*, 35.
[16] a) H.-J. Sass, S. A. Mueller, G. Bueldt, A. Engel, *J. Mol. Biol.* **1999**, *285*, 1903; b) S. Scheuring, J. Seguin, S. Marco, D. Levy, B. Robert, J. L. Rigaud, *Proc. Natl. Acad. Sci. USA* **2003**, *100*, 1690.
[17] T. Yang, O. K. Baryshnikova, H. Mao, M. A. Holden, P. S. Cremer, *J. Am. Chem. Soc.* **2003**, *125*, 4779.
[18] M. Radmacher, R. W. Tillamnn, M. Fritz, H. E. Gaub, *Science* **1992**, *257*, 1900.
[19] C. Das, K. Sheikh, P. Olmsted, S. Connell, *Phys. Rev. E: Stat., Nonlinear, Soft Matter Phys.* **2010**, *82*.
[20] D. M. Engelman, *Nature* **2005**, *438*, 578.
[21] S. Bahatyrova, R. N. Frese, C. A. Siebert, J. D. Olsen, K. van der Werf, R. van Grondelle, R. A. Niederman, P. A. Bullough, C. Otto, C. N. Hunter, *Nature* **2004**, *430*, 1058.
[22] S. Scheuring, *Curr. Opin. Chem. Biol.* **2006**, *10*, 387.
[23] a) P. G. Adams, D. J. Mothersole, I. W. Ng, J. D. Olsen, C. N. Hunter, *Biochim. Biophys. Acta, Bioenerg.* **2011**, *1807*, 1044; b) E. C. Ratcliffe, R. B. Tunnicliffe, I. W. Ng, P. G. Adams, P. Qian, K. Holden-Dye, M. R. Jones, M. P. Williamson, C. N. Hunter, *Biochim. Biophys. Acta, Bioenerg.* **2011**, *1807*, 95; c) I. W. Ng, P. G. Adams, D. J. Mothersole, C. Vasilev, E. C. Martin, H. P. Lang, J. D. Tucker, C. N. Hunter, *Biochim. Biophys. Acta, Bioenerg.* **2011**, *1807*, 1056.
[24] P. G. Adams, C. N. Hunter, *Biochim. Biophys. Acta, Bioenerg.* **2012**, *1817*, 1616.
[25] a) M. Bally, K. Bailey, K. Sugihara, D. Grieshaber, J. Voros, B. Stadler, *Small* **2010**, *6*, 2481; b) E. T. Castellana, P. S. Cremer, *Surf. Sci. Rep.* **2006**, *61*, 429; c) M. Eeman, M. Deleu, *Biotechnol., Agron., Soc. Environ.* **2010**, *14*, 719.
[26] M. P. Goertz, N. Goyal, G. A. Montaño, B. C. Bunker, *Langmuir* **2011**, *27*, 5481.
[27] E. Reimhult, K. Kumar, *Trends Biotechnol.* **2008**, *26*, 82.
[28] H. Mukundan, D. N. Price, M. Goertz, R. Parthasarathi, G. A. Montaño, S. Kumar, M. R. Scholfield, A. S. Anderson, S. Gnanakaran, S. Iyer, J. Schmidt, B. I. Swanson, *Tuberculosis* **2012**, *92*, 38.
[29] a) D. Pum, G. Stangl, C. Sponer, K. Riedling, P. Hudek, W. Fallmann, U. B. Sleytr, *Proceedings of International Conference on Micro- and Nanofabrication* **1997**, 297; b) S. Y. Qi, J. T. Groves, A. K. Chakraborty, *Proc. Natl. Acad. Sci. USA* **2001**, *98*, 6548; c) T. L. Yang, S. Y. Jung, H. B. Mao, P. S. Cremer, *Anal. Chem.* **2001**, *73*, 165; d) K. Yuyama, N. Sekino-Suzuki, Y. Sanai, K. Kasahara, *Trends Glycosci. Glycotechnol.* **2003**, *15*, 139.
[30] a) P. A. Bullough, P. Qian, C. N. Hunter, in *The Purple Phototrophic Bacteria* (Eds: C. N. Hunter, F. Daldal, M. C. Thurnauer, J. T. Beatty), Springer, Dordrecht, The Netherlands **2009**, Ch. *9*; b) R. N. Frese, C. A. Siebert, R. A. Niederman, C. N. Hunter, C. Otto, R. van Grondelle, *Proc. Natl. Acad. Sci. USA* **2004**, *101*, 17994; c) S. Scheuring, T. Boudier, J. N. Sturgis, *J. Struct. Biol.* **2007**, *159*, 268; d) S. Scheuring, J. N. Sturgis, *Photosynth. Res.* **2009**, *102*, 197; e) J. N. Sturgis, J. D. Tucker, J. D. Olsen, C. N. Hunter, R. A. Niederman, *Biochemistry* **2009**, *48*, 3679.
[31] K. El Kirat, S. Morandat, Y. F. Dufrêne, *Biochim. Biophys. Acta, Biomembr.* **2010**, *1798*, 750.
[32] J. Zhong, D. He, *Chem. Eur. J.* **2012**, *18*, 4148.
[33] J. N. L. Albert, T. H. Epps III, *Mater. Today* **2010**, *13*, 24.
[34] S. Belegrinou, J. Dorn, M. Kreiter, K. Kita-Tokarczyk, E.-K. Sinner, W. Meier, *Soft Matter* **2010**, *6*, 179.
[35] J. Y. Cheng, C. A. Ross, H. I. Smith, E. L. Thomas, *Adv. Mater.* **2006**, *18*, 2505.
[36] S. B. Darling, *Prog. Polym. Sci.* **2007**, *32*, 1152.
[37] M. P. Goertz, L. E. Marks, G. A. Montaño, *ACS Nano* **2012**, *6*, 1532.
[38] A. Gonzalez-Perez, V. Castelletto, I. W. Hamley, P. Taboada, *Soft Matter* **2011**, *7*, 1129.
[39] N. Kumar, J.-i. Hahm, *Langmuir* **2005**, *21*, 6652.
[40] S. Santer, A. Kopyshev, H.-K. Yang, J. Rühe, *Macromolecules* **2006**, *39*, 3056.
[41] M. Grandbois, H. Clausen-Schaumann, H. Gaub, *Biophys. J.* **1998**, *74*, 2398.
[42] M.-C. Giocondi, D. Yamamoto, E. Lesniewska, P.-E. Milhiet, T. Ando, C. Le Grimellec, *Biochim. Biophys. Acta, Bioenerg.* **2010**, *1798*, 703.
[43] A. Ponnuswamy, J. Nulton, J. M. Mahaffy, P. Salamon, T. G. Frey, A. R. C. Baljon, *Phys. Biol.* **2005**, *2*, 73.
[44] a) L. R. Cambrea, J. S. Hovis, *Biophys. J.* **2007**, *92*, 3587; b) K. Giger, E. R. Lamberson, J. S. Hovis, *Langmuir* **2009**, *25*, 71.
[45] L. R. Cambrea, F. Haque, J. L. Schieler, J.-C. Rochet, J. S. Hovis, *Biophys. J.* **2007**, *93*, 1630.
[46] R. Parthasarathy, C.-h. Yu, J. T. Groves, *Langmuir* **2006**, *22*, 5095.
[47] M. Sundh, S. Svedhem, D. S. Sutherland, *J. Phys. Chem. B* **2011**, *115*, 7838.
[48] J. H. Werner, G. A. Montaño, A. L. Garcia, N. A. Zurek, E. A. Akhadov, G. P. Lopez, A. P. Shreve, *Langmuir* **2009**, *25*, 2986.
[49] R. Zeineldin, J. A. Last, A. L. Slade, L. K. Ista, P. Bisong, M. J. O'Brien, S. R. J. Brueck, D. Y. Sasaki, G. P. Lopez, *Langmuir* **2006**, *22*, 8163.
[50] a) N. Ahamad, D. Prezgot, A. Ianoul, *J. Nanopart. Res.* **2012**, *14*, 724; b) S. Hong, P. R. Leroueil, E. K. Janus, J. L. Peters, M.-M. Kober, M. T. Islam, B. G. Orr, J. R. Baker Jr, M. M. B. Holl, *Bioconjugate Chem.* **2006**, *17*, 728; c) P. R. Leroueil, S. A. Berry, K. Duthie, G. Han, V. M. Rotello, D. Q. McNerny, J. R. Baker Jr, B. G. Orr, M. M. B. Holl, *Nano Lett.* **2008**, *8*, 420; d) Y. Roiter, M. Ornatska, A. R. Rammohan, J. Balakrishnan, D. R. Heine, S. Minko, *Langmuir* **2009**, *25*, 6287; e) J. W. Taylor, L. K. Kurihara, L. J. Martinez-Miranda, *Appl. Phys. Lett.* **2012**, *100*, 173115.
[51] S. C. Hayden, G. Zhao, K. Saha, R. L. Phillips, X. Li, O. R. Miranda, V. M. Rotello, M. A. El-Sayed, I. Schmidt-Krey, U. H. F. Bunz, *J. Am. Chem. Soc.* **2012**, *134*, 6920.

[52] M. Schulz, A. Olubummo, W. H. Binder, *Soft Matter* **2012**, *8*, 4849.
[53] A. Verma, F. Stellacci, *Small* **2010**, *6*, 12.
[54] a) M. D. Chavanpatil, A. Khdair, J. Panyam, *J. Nanosci. Nanotechnol.* **2006**, *6*, 2651; b) Y. Fukumori, H. Ichikawa, *Adv. Powder Technol.* **2006**, *17*, 1; c) R. H. Mueller, *Adv. Drug Delivery Rev.* **2007**, *59*, 375; M. Soloviev, *J. Nanobiotechnol.* **2007**, *5*, 11; d) J. C. Sung, B. L. Pulliam, D. A. Edwards, *Trends Biotechnol.* **2007**, *25*, 563; e) O. Veiseh, J. W. Gunn, M. Zhang, *Adv. Drug Delivery Rev.* **2010**, *62*, 284; f) C. Wei, *J. Nanosci. Nanotechnol.* **2008**, *8*, 1019; g) P. J. A. De Jong Wh Fau - Borm, P. J. Borm, *Int. J. Nanomed.* *3*, 133.
[55] W. Bo, Z. Liangfang, B. Sung Chul, S. Granick, *Proc. Natl. Acad. Sci. USA* **2008**, *105*, 18171.
[56] a) E. C. Cho, L. Au, Q. Zhang, Y. Xia, *Small* **2010**, *6*, 517; b) M. R. R. de Planque, S. Aghdaei, T. Roose, H. Morgan, *ACS Nano* **2011**, *5*, 3599; c) B. Jing, Y. Zhu, *J. Am. Chem. Soc.* **2011**, *133*, 10983; d) X. Yi, X. Shi, H. Gao, *Phys. Rev. Lett.* **2011**, *107*, 098101.
[57] M. P. Goertz, N. Goyal, B. C. Bunker, G. A. Montaño, *J. Colloid Interface Sci.* **2011**, *358*, 635.
[58] X. Xiao, G. A. Montaño, A. Allen, K. E. Achyuthan, D. R. Wheeler, S. M. Brozik, *Langmuir* **2011**, *27*, 9484.
[59] X. Xiao, G. A. Montaño, T. L. Edwards, A. Allen, K. E. Achyuthan, R. Polsky, D. R. Wheeler, S. M. Brozik, *Langmuir* **2012**, *28*, 17396.
[60] H. Zhang, J. Joubert, S. Saavedra, *Adv. Polym. Sci.* **2010**, *224*, 1–42.
[61] C. C. Hayden, J. S. Hwang, E. A. Abate, M. S. Kent, D. Y. Sasaki, *J. Am. Chem. Soc.* **2009**, *131*, 8728.
[62] G. Krausch, R. Magerle, *Adv. Mater.* **2002**, *14*, 1579.
[63] a) I. In, Y.-H. La, S.-M. Park, P. F. Nealey, P. Gopalan, *Langmuir* **2006**, *22*, 7855; b) H. M. Kang, A. Mangham, M. P. Stoykovich, R. J. Hamers, P. F. Nealey, *Abstr. Pap. Am. Chem. Soc.* **2007**, *233*; c) S. M. Park, M. P. Stoykovich, R. Ruiz, Y. Zhang, C. T. Black, P. E. Nealey, *Adv. Mater.* **2007**, *19*, 607.
[64] B. Zhao, W. J. Brittain, *Prog. Polym. Sci.* **2000**, *25*, 677.
[65] D. Usov, V. Gruzdev, M. Nitschke, M. Stamm, O. Hoy, I. Luzinov, I. Tokarev, S. Minko, *Macromolecules* **2007**, *40*, 8774.
[66] a) S. Minko, D. Usov, E. Goreshnik, M. Stamm, *Macromol. Rapid Commun.* **2001**, *22*, 206; b) A. Sidorenko, S. Minko, K. Schenk-Meuser, H. Duschner, M. Stamm, *Langmuir* **1999**, *15*, 8349.
[67] M. Lemieux, D. Usov, S. Minko, M. Stamm, H. Shulha, V. V. Tsukruk, *Macromolecules* **2003**, *36*, 7244.
[68] S. A. Prokhorova, A. Kopyshev, A. Ramakrishnan, H. Zhang, J. Ruhe, *Nanotechnol.* **2003**, *14*, 1098.
[69] A. D. Price, S.-M. Hur, G. H. Fredrickson, A. L. Frischknecht, D. L. Huber, *Macromolecules* **2011**, *45*, 510.
[70] M. R. Bockstaller, Y. Lapetnikov, S. Margel, E. L. Thomas, *J. Am. Chem. Soc.* **2003**, *125*, 5276.
[71] U. Y. Jeong, H. C. Kim, R. L. Rodriguez, I. Y. Tsai, C. M. Stafford, J. K. Kim, C. J. Hawker, T. P. Russell, *Adv. Mater.* **2002**, *14*, 274.
[72] C. B. Tang, E. M. Lennon, G. H. Fredrickson, E. J. Kramer, C. J. Hawker, *Science* **2008**, *322*, 429.
[73] S. B. Darling, N. A. Yufa, A. L. Cisse, S. D. Bader, S. J. Sibener, *Adv. Mater.* **2005**, *17*, 2446.
[74] G. Liu, J. Zhao, *Langmuir* **2006**, *22*, 2923.
[75] N. Kumar, O. Parajuli, A. Dorfman, D. Kipp, J.-i. Hahm, *Langmuir* **2007**, *23*, 7416.
[76] G. Riess, *Prog. Polym. Sci.* **2003**, *28*, 1107.
[77] O. Onaca, R. Enea, D. W. Hughes, W. Meier, *Macromol. Biosci.* **2009**, *9*, 129.
[78] K. Yu, A. Eisenberg, *Macromolecules* **1998**, *31*, 3509.
[79] a) D. E. Discher, F. Ahmed, *Annu. Rev. Biomed. Eng.* **2006**, *8*, 323; b) D. E. Discher, V. Ortiz, G. Srinivas, M. L. Klein, Y. Kim, D. David, S. Cai, P. Photos, F. Ahmed, *Prog. Polym. Sci.* **2007**, *32*, 838.
[80] J. Dorn, S. Belegrinou, M. Kreiter, E.-K. Sinner, W. Meier, *Macromol. Biosci.* **2011**, *11*, 514.
[81] D. P. Shepherd, K. J. Whitcomb, K. K. Milligan, P. M. Goodwin, M. P. Gelfand, A. Van Orden, *J. Phys. Chem. C* **2010**, *114*, 14831.